EJN
European Journal of Neuroscience

European Journal of Neuroscience, Vol. 28, pp. 1301–1315, 2008 doi:10.1111/j.1460-9568.2008.06437.x

NEUROSYSTEMS

Temporally structured replay of neural activity in a model of entorhinal cortex, hippocampus and postsubiculum

Michael E. Hasselmo
Center for Memory and Brain, Department of Psychology and Program in Neuroscience, Boston University, 2 Cummington St, Boston, MA 02215, USA

Keywords: episodic memory, grid cells, head direction cells, memory retrieval, postsubiculum, rat

Abstract

The spiking activity of hippocampal neurons during rapid eye movement (REM) sleep exhibits temporally structured replay of spiking occurring during previously experienced trajectories. Here, temporally structured replay of place cell activity during REM sleep is modeled in a large-scale network simulation of grid cells, place cells and head direction cells. During simulated waking behavior, the movement of the simulated rat drives activity of a population of head direction cells that updates the activity of a population of entorhinal grid cells. The population of grid cells drives the activity of place cells coding individual locations. Associations between location and movement direction are encoded by modification of excitatory synaptic connections from place cells to speed modulated head direction cells. During simulated REM sleep, the population of place cells coding an experienced location activates the head direction cells coding the associated movement direction. Spiking of head direction cells then causes frequency shifts within the population of entorhinal grid cells to update a phase representation of location. Spiking grid cells then activate new place cells that drive new head direction activity. In contrast to models that perform temporally compressed sequence retrieval similar to sharp wave activity, this model can simulate data on temporally structured replay of hippocampal place cell activity during REM sleep at time scales similar to those observed during waking. These mechanisms could be important for episodic memory of trajectories.

Introduction

Neurophysiological data from the hippocampus demonstrates that spiking activity of place cells during rapid eye movement (REM) sleep shows temporally structured replay of sequences that occurred during prior waking behavior (Louie & Wilson, 2001). This replay occurs at time scales similar to those during waking (Louie & Wilson, 2001). Recordings during REM periods of 60–240-s duration (mean 114 s) showed temporal scaling factors ranging from 0.55 to 2.49 (mean 1.4). A scaling factor of 1.0 means replay occurs at the same speed as waking, and a scaling factor of 1.4 means a 60-s period of REM matches a 43-s period of waking. Other studies have also shown neural replay of previously experienced trajectories during waking (Foster & Wilson, 2006; Diba & Buzsaki, 2007; Johnson & Redish, 2007) and slow wave sleep (Skaggs & McNaughton, 1996; Lee & Wilson, 2002), but non-REM replay involves retrieval at a very compressed time scale.

Previous models have simulated the replay of sequences at a compressed time scale (Jensen & Lisman, 1996a,b; Levy, 1996; Tsodyks *et al.*, 1996; Wallenstein & Hasselmo, 1997; Hasselmo & Eichenbaum, 2005). Fast replay occurs because associations are formed directly between place cells representing sensory states, and the time window of modification of synapses during encoding is longer than the time scale of synaptic transmission during retrieval. In contrast, the model presented here forms associations between place cells coding sensory state and head direction cells coding the action leading to the next state. Persistent spiking in head direction cells allows updating of a continuous representation of space provided by modelled grid cells. The combination of persistent firing and a continuous representation of space and actions allows simulation of the slower temporally structured replay observed during REM sleep.

Beyond the REM data (Louie & Wilson, 2001), this model was motivated by neurophysiological data showing: (1) grid cell firing patterns in entorhinal cortex (Hafting *et al.*, 2005; Sargolini *et al.*, 2006; Fyhn *et al.*, 2007), (2) membrane potential oscillations in entorhinal cortex layer II (Alonso & Llinas, 1989; Dickson *et al.*, 2000; Giocomo *et al.*, 2007), (3) persistent firing in deep entorhinal cortex neurons (Egorov *et al.*, 2002; Fransén *et al.*, 2006) and postsubiculum (Yoshida & Hasselmo, 2008), (4) place cells in hippocampus (O'Keefe, 1976; O'Keefe & Burgess, 2005; McNaughton *et al.*, 2006) and (5) head direction cells in the postsubiculum (Taube *et al.*, 1990b; Sharp *et al.*, 2001; Taube & Bassett, 2003) and deep layers of entorhinal cortex (Sargolini *et al.*, 2006). Data on differences in membrane potential oscillation frequency along the dorsal to ventral axis of entorhinal cortex (Giocomo *et al.*, 2007) support the model of grid cells used here, in which grid cell oscillation phase integrates head direction input to code continuous space

Correspondence: Dr M. E. Hasselmo, as above.
E-mail: hasselmo@bu.edu

Received 12 February 2008, revised 31 July 2008, accepted 4 August 2008

(Burgess *et al.*, 2007; Hasselmo *et al.*, 2007). Graded persistent firing occurs in deep entorhinal neurons during cholinergic modulation (Egorov *et al.*, 2002), consistent with acetylcholine levels observed during waking and REM sleep (Marrosu *et al.*, 1995). Persistent firing could allow deep entorhinal or postsubicular head direction cells to hold activity scaled to the speed and direction of retrieved movement to update the phase of grid cell oscillations. These cellular mechanisms allow an explicit representation of the time duration of sequences during retrieval, providing the temporally structured replay seen during REM sleep (Louie & Wilson, 2001). These simulations generate predictions about replay of grid cell and head direction cell activity during REM sleep.

Methods

The temporally structured replay of place cell activity during REM sleep was simulated in a network model summarized in Fig. 1. This model includes a population of grid cells based on data from recordings in the medial entorhinal cortex (Hafting *et al.*, 2005; Sargolini *et al.*, 2006; Fyhn *et al.*, 2007). Grid cells were generated using a recent model of potential mechanisms for grid cell formation (Burgess *et al.*, 2007; Giocomo *et al.*, 2007; Hasselmo *et al.*, 2007), as shown in Fig. 2 for open field activity and Fig. 3 for a circular track. The model also includes a population of place cells with place fields resembling data from recordings on linear tracks (Louie & Wilson, 2001; Lee *et al.*, 2004a,b). Place cells were generated using input from grid cells in a manner similar to other models (Fuhs & Touretzky, 2006; McNaughton *et al.*, 2006; Rolls *et al.*, 2006; Solstad *et al.*, 2006; Franzius *et al.*, 2007b; Molter & Yamaguchi, 2007). Place cell activity in the network is shown in Fig. 4. Finally, the model includes a population of head direction cells based on neural activity recorded in deep layers of the entorhinal cortex (Sargolini *et al.*, 2006) or postsubiculum (dorsal presubiculum) (Taube *et al.*, 1990a, 1996; Taube & Burton, 1995; Sharp, 1996; Sharp *et al.*, 2001; Taube & Bassett, 2003), as shown in Fig. 5. The simulation of behavior will be described first, followed by description of the simulation of activity in different populations of neurons, followed by description of the mechanisms of encoding during waking due to synaptic modification, and finally the mechanism of retrieval during REM sleep.

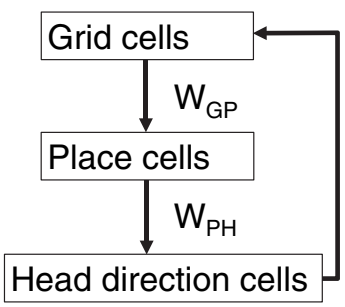

FIG. 1. Proposed episodic memory circuit for encoding and REM replay of trajectories using grid cells, place cells and head direction cells. Grid cells in medial entorhinal cortex (EC) are generated by speed-modulated head direction input. The grid cells drive place cell firing in the hippocampus via synapses W_{GP}. During waking (encoding), links between state (place) and action (speed modulated head direction) are made by strengthening synapses W_{PH} between place cells and head direction cells. During retrieval, activity of place cells activates the associated head direction cells representing velocity. The head direction cells then update grid cells to activate place cells representing the next encoded location.

Behavior on circular track

The temporally structured replay of place cell spiking activity during REM sleep was demonstrated in an experiment using a circular

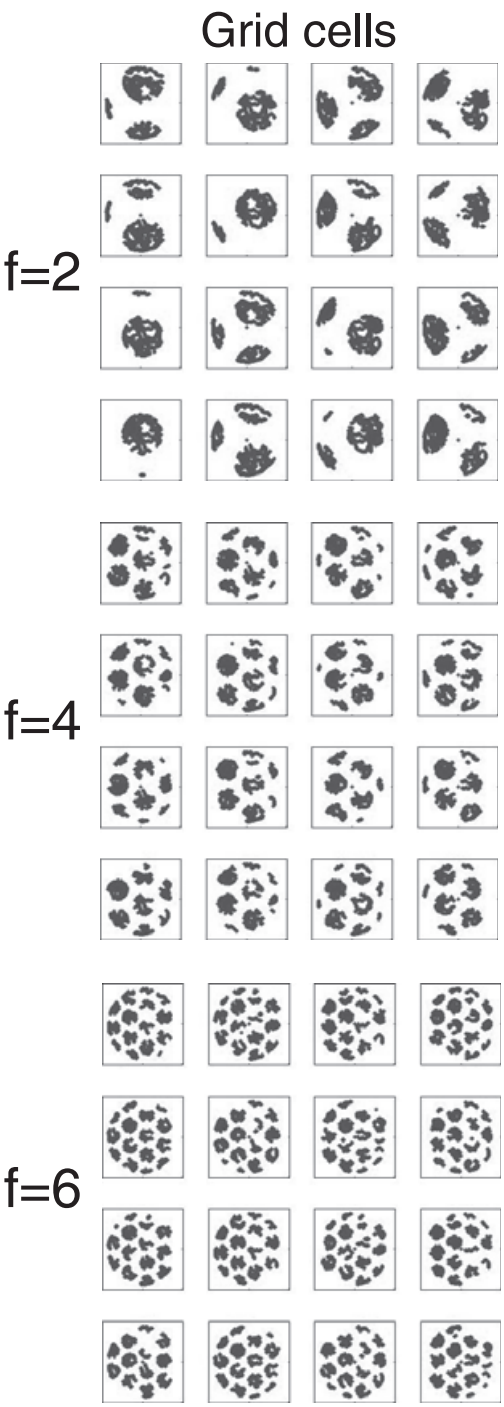

FIG. 2. Example of grid cell firing in the simulation. The model used a population of 75 grid cells. Here, the spatial periodicity of grid cell firing is illustrated in a smaller population of 48 grid cells during random foraging in an open field environment (trajectory from Hafting et al. 2005). Each square shows the pattern of firing of one simulated grid cell during the same open field trajectory. Firing fields are made up of many gray dots indicating the location of the virtual rat when the grid cell fires. Grid cells differ by baseline frequency in the top ($f = 2$), middle ($f = 4$) and bottom ($f = 6$) groups. Within each group, grid cells differ by initial phase of oscillation, with phase $\varphi = 0$, $\pi/2$, π and $3\pi/2$. These simulations use the same orientation of $\phi = 0$.

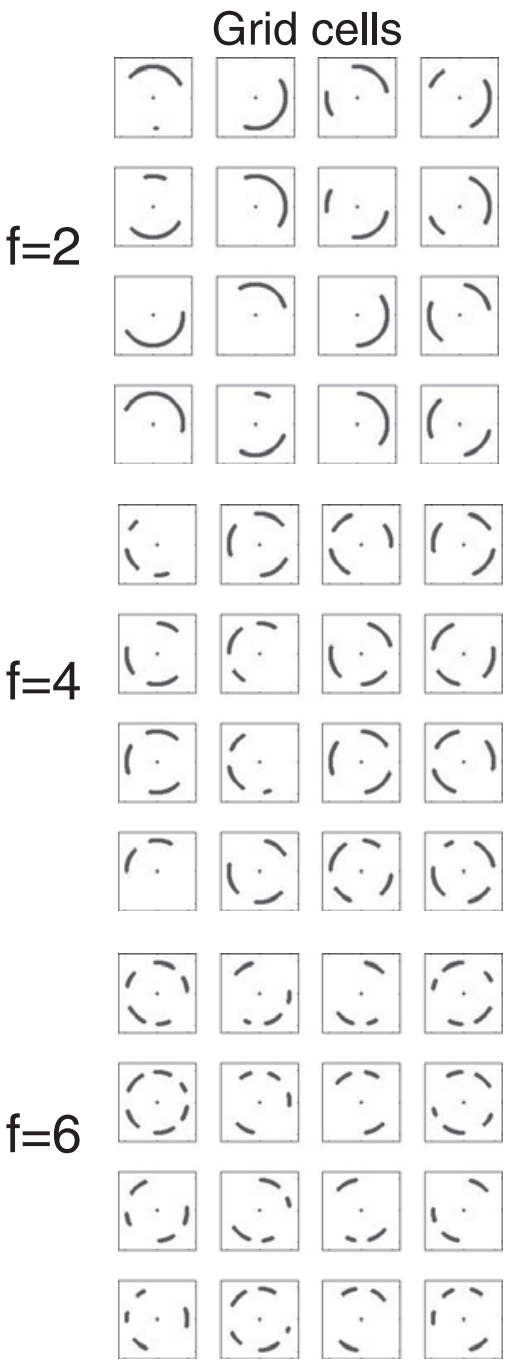

FIG. 3. Example of activity in the population of grid cells during running on the circular track. Each square shows the pattern of firing of one simulated grid cell during running on the circular track. Firing fields are made up of gray dots indicating location when grid cell fires. Grid cells differ by baseline frequency $f = 2$, 4 and 6 in groups. Within groups, grid cells differ by initial phase, with phase $\varphi = 0$, $\pi/2$, π and $3\pi/2$. As in Fig. 2, orientation $\phi = 0$.

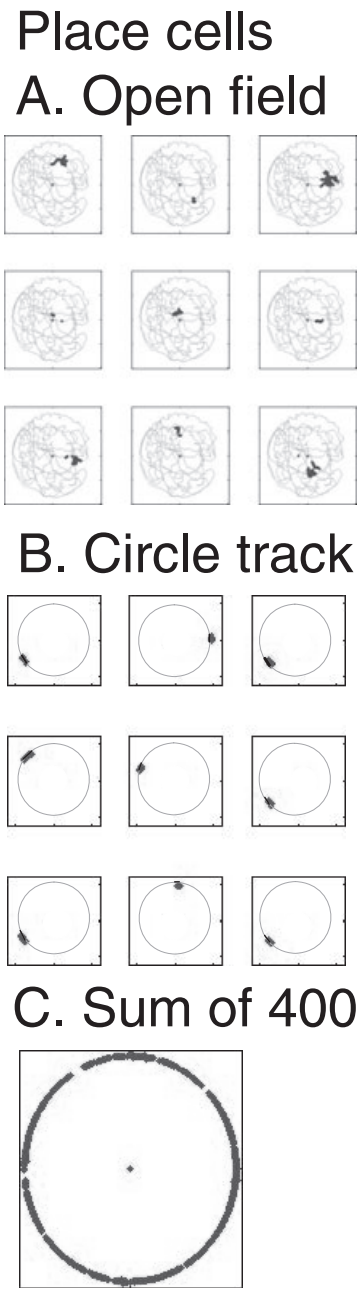

FIG. 4. Example of place cell firing in the simulation. The full simulation used 400 place cells. (A) Examples of spiking activity of nine place cells in an open field during a complex foraging trajectory (shown in gray). Black dots indicate location of rat when place cell fires. (B) Example of nine place cells during running on the circular track. Dots indicating location of the virtual rat when individual cells fired. Place cells fired in localized regions of the circular track. (C) Simultaneous plot of the spiking activity of all 400 cells, showing that spikes occurred in individual place cells for almost all locations on the circular track.

running track (Louie & Wilson, 2001). Therefore, the simulations presented here focus on the virtual rat running a circular trajectory during waking (encoding). This was simulated by starting a virtual rat running south at a fixed rate, and then modulating the velocity vector of running so that the rat would run around a circle with a diameter of 95 cm, matching the experimental apparatus. Unless otherwise noted, the virtual rat ran at a mean speed of 50 cm/s for 24 s, resulting in a total arc length of 1200 cm, or about four cycles of the approximately 300-cm circumference of the circular track, but effects of variation in speed were also tested. After simulation of running in the circular track, the simulation was shifted to the REM sleep mode with no external input, and temporally structured replay was tested by reactivation of the pattern of grid cell, place cell and head direction cell activity from the first step of waking.

Grid cell model

Consistent with experimental data, the population of grid cells in the model includes neurons that fire with different size and spacing

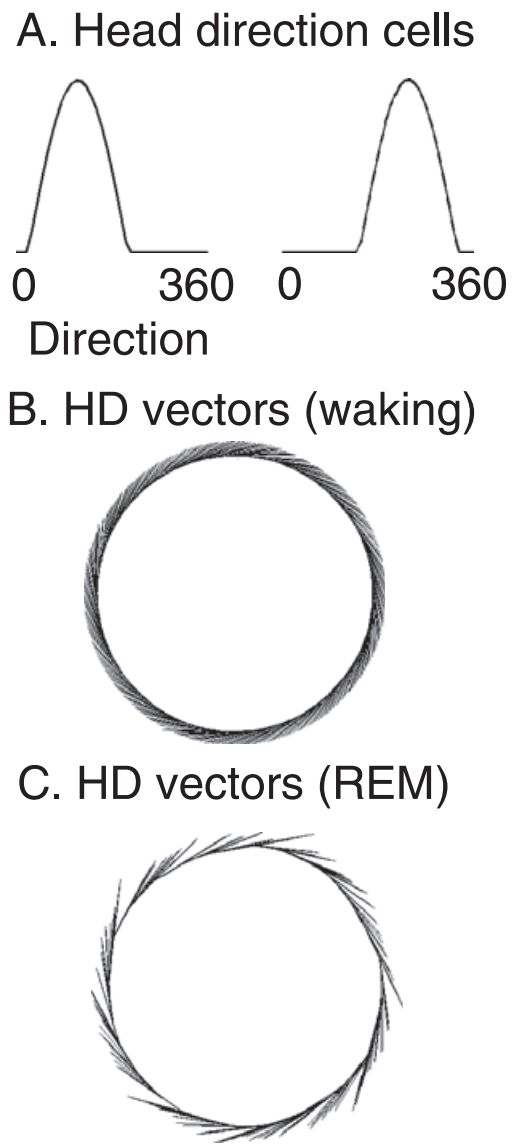

FIG. 5. (A) Example of tuning of two head direction cells from the simulation, with preference for angles of 120° and 240°. (B–C) Movement directions coded by the population of head direction cells during running on the circular track (95 cm in diameter). Straight lines show the velocity vectors coded by head direction at each location. (B) During waking (encoding), head direction cells driven by actual movement effectively code direction at each point in time, resulting in similar length and gradual shift in orientation of lines (for clarity, lines are shown for every 5th time step). (C) During REM replay (retrieval), head direction cells are activated by the spread of activity from place cells. This results in retrieved velocity vectors that vary somewhat in length and orientation, but effectively retrieve the circular trajectory (lines are shown for every time step).

between firing fields, as well as different spatial phases relative to the environment. Orientation was kept consistent within a simulation, based on similarity of orientation within each local region of entorhinal cortex. These properties are obtained with the Burgess, Barry and O'Keefe model of grid cells (Burgess *et al.*, 2005, 2007; O'Keefe & Burgess, 2005). In this model, membrane potential oscillations in individual neurons interfere in a manner resulting in grid cell firing patterns. The difference in size and spacing of grid fields results from differences in the baseline frequency of membrane potential oscillations, consistent with experimental data showing differences in intrinsic membrane potential oscillation frequency along the dorsal to ventral axis of the medial entorhinal cortex (Giocomo *et al.*, 2007; Hasselmo *et al.*, 2007).

Data show that the frequency of membrane potential oscillations is increased from baseline by depolarizing input (Alonso & Llinas, 1989; Alonso & Klink, 1993; Dickson *et al.*, 2000; Giocomo *et al.*, 2007). Thus, depolarizing input to superficial layers of entorhinal cortex (Caballero-Bleda & Witter, 1993) from head direction cells in the postsubiculum (Taube *et al.*, 1990b; Sharp *et al.*, 2001; Taube & Bassett, 2003) and deep layers of entorhinal cortex (Sargolini *et al.*, 2006) could provide changes in oscillation frequency dependent upon head direction activity. In the Burgess model, speed-modulated head direction input alters oscillation frequency in different dendrites of entorhinal stellate cells in proportion to the speed of movement in different directions (Burgess *et al.*, 2007; Giocomo *et al.*, 2007; Hasselmo *et al.*, 2007). The pattern of grid cell firing $g(t)$ arises due to interference of different frequencies induced by the integration of different head direction inputs. The model used in previous papers is described here by the following equation:

$$g_{jk}(t) = \Theta[\prod_i \{\cos(2\pi f_j t) + \cos((2\pi f_j (t + B \int_0^t \vec{h}_i(\tau)\mathrm{d}\tau) + \vec{\varphi}_{ik})\}] \quad (1)$$

In this equation, $g_{jk}(t)$ represents the firing over time of a single grid cell with baseline frequency f_j and the dendritic oscillation phase vector $\vec{\varphi}_{ik}$. Π_i represents the product of the different dendritic oscillations receiving input from different components of the head direction vector with index i. Θ represents a Heaviside step function output (the model has output 1 for values above a threshold of 0.3, and output of 0 otherwise). The intrinsic membrane potential oscillations have baseline frequency f_j for different populations of grid cells j. The frequencies of dendritic oscillations are modulated by input from a population of head direction cells with activity represented by the vector $\vec{h}_i(t)$. This representation of head direction is described below and is mathematically equivalent to the Burgess model. This input is scaled by a constant B set to 0.00385 based on experimental data (Giocomo *et al.*, 2007). The dendritic branches of a single grid cell have initial phases represented by the initial phase vector $\vec{\varphi}_{ik}$ that has an element for each component of input h_i and differs across individual grid cells k.

This model creates grid cell firing fields with spacing dependent upon modulation of the intrinsic oscillation frequency f_j (Giocomo *et al.*, 2007; Hasselmo *et al.*, 2007). The sum of the somatic oscillation with frequency f and each dendritic oscillation with frequency $f + fB\vec{h}(t)$ results in an interference pattern that has an envelope with a frequency equal to the difference of the two frequencies $fB\vec{h}(t)$. Note that this model can also generate grid cell patterns with direct interactions of dendritic oscillations in the absence of somatic oscillations (Hasselmo *et al.*, 2007). Recent simulations show that dendritic oscillations tend to synchronize, but the same model presented here can be implemented by using neurons that show intrinsic persistent spiking at a stable frequency and can shift their phase transiently in response to depolarizing input (Hasselmo, 2008; Hasselmo & Brandon, 2008). This is consistent with extensive experimental data on properties of persistent spiking neurons in entorhinal cortex (Egorov *et al.*, 2002; Fransén *et al.*, 2006). That implementation uses changes in spiking phase caused by transient input but does not use long-term changes in stable persistent spiking frequency caused by stronger input.

In most simulations presented here, the model in Eqn 1 was replaced with Eqn 2, which generates denser grid cell firing and more

effective place cell formation. This gave function similar to Eqn 1 with less variability in spike timing.

$$g_{jk}(t) = \Theta[\prod_i \cos(2\pi f_j B \int_0^t \vec{h}_i(\tau)\mathrm{d}\tau + \vec{\varphi}_{ik})] \quad (2)$$

These models of grid cells generate grid cell firing patterns that depend on three parameters. The size and spacing of firing fields depends upon parameter f_j, the spatial phase depends upon $\vec{\varphi}_{ik}$ and the orientation depends upon the parameter ϕ_i (described in the section on head direction input). Examples of grid cell firing activity are shown for random foraging in an open field in Fig. 2. For ease of viewing, only 48 cells are shown in Figs 2 and 3. In Fig. 3, firing patterns are shown for the same grid cell model during simulated running of a circular track during waking. Grid cell patterns similar to those on the circular track in Fig. 3 provided the input for encoding in these simulations. The simulations presented here all used 75 grid cells (25 grid cells at each frequency, with five different spatial phases in each spatial dimension).

Note that the function of the model presented here can be obtained with different types of grid cell models, as long as they perform path integration based on head direction activity. Thus, the model can also function with grid cell models using interactions between neurons spiking at different phases (Hasselmo, 2008; Hasselmo & Brandon, 2008), and with continuous attractor models updated by head direction input (Fuhs & Touretzky, 2006; McNaughton *et al.*, 2006).

Place cells

The next stage of the model involves the generation of place cell spiking activity based on grid cell spiking activity. Previous research has proposed different ways by which place cells could arise from grid cell input (Fuhs & Touretzky, 2006; McNaughton *et al.*, 2006; Rolls *et al.*, 2006; Solstad *et al.*, 2006; Franzius *et al.*, 2007b; Molter & Yamaguchi, 2007). The mechanism used here resembles previous models, and was selected for simplicity and computation speed. In the model presented here, a simple thresholded summation of the location-dependent firing properties of entorhinal grid cells is used for the initial induction of place cell activity. A wide array of grid cells with different spatial phases and frequencies are simulated. Place cells are then created during a period before simulation of waking (encoding) and REM replay. During this period, random subsets of three grid cells are selected as inputs for a new place cell that fires in any location where all three grid cells fire. This generates a spatial firing pattern for each place cell that is evaluated by taking the standard deviation of spiking location in the x and y dimension. If the standard deviation of spiking location is smaller than a previously set parameter in both dimensions, then this place cell is selected for inclusion. The input synapses from the randomly selected subset of three grid cells to this place cell are strengthened according to the outer product equation:

$$W_{\mathrm{GP}} = \sum \vec{g}(t)^T \vec{p}(t) \quad (3)$$

where $\vec{g}(t)^T$ is a column vector of presynaptic grid cell activity including the three currently selected grid cells, and $\vec{p}(t)$ is a row vector of place cell activity with only the currently selected place cell active. This ensures that the same place cells are reliably activated in the same location dependent on the pattern of grid cell spiking induced by the phase of grid cells.

During both waking (encoding) and REM replay, the place cell row vector $\vec{p}(t)$ results from the pattern of activity in the grid cell row vector $\vec{g}(t)$dependent upon multiplication by the previously modified synaptic connectivity W_{GP} between these regions as follows:

$$\vec{p}(t) = \vec{g}(t) W_{\mathrm{GP}} \quad (4)$$

Examples of individual place cells from the simulation are shown for an open field trajectory in Fig. 4A and for the circular track in Fig. 4B. The coverage of the circular track by the firing fields of 400 place cells is shown in Fig. 4C, illustrating that this number of place cells effectively represents location throughout the circular track. Most simulations presented here used 400 place cells, except where the effect of number of place cells on REM replay is tested.

The responses of the grid cells and place cells in this model are not direction dependent, consistent with data from recordings in the open field. However, if the grid cell oscillation phase is reset at the reward location, the response of grid cells (and therefore also of place cells) will be directional. Alternatively, if the grid cell phase is updated by running speed alone without head direction, then the grid cells will respond on the basis of the arc length of the trajectory, rather than two-dimensional location. In both of these conditions, if the rat were tested with a different direction of running, the firing pattern of grid cells and place cells would differ. This might enhance the capacity to encode overlapping trajectories without interference (Hasselmo, 2007).

Head direction cell activity

The representation of movement direction (velocity) in the model is provided by head direction cells. Extensive experimental data describe head direction cells in the deep layers of the entorhinal cortex (Sargolini *et al.*, 2006) and in other areas including the postsubiculum (dorsal presubiculum) and the anterior thalamus (Taube *et al.*, 1990a, 1996; Knierim *et al.*, 1995, 1998; Taube & Burton, 1995; Sharp, 1996; Sharp *et al.*, 2001; Taube & Bassett, 2003; Yu *et al.*, 2006). Head direction cells fire selectively when the rat is heading in angles close to the preferred direction of the cell. In the model, the activity of head direction cells is modulated by the speed of the simulated rat. Physiologically, this could arise from input from cells showing firing rate changes with translational speed in deep entorhinal layers (Sargolini *et al.*, 2006) and in postsubiculum (Taube *et al.*, 1990b; Sharp, 1996). Alternatively, the speed modulation could also arise due to modulation from neurons in other regions that respond linearly to different speeds of translational motion (Sharp, 1996; O'Keefe *et al.*, 1998; Sharp & Turner-Williams, 2005; Sharp *et al.*, 2006).

This model simulates the activity of multiple head direction cells that are modulated by speed. Head direction cell activity is represented by the vector $\vec{h}(t)$. The model computes the speed-modulated head direction response from the velocity vector of movement in space $\vec{v}(t) = [\Delta x(t), \Delta y(t)]$ that combines the distance moved in the x and y directions during each discrete unit of time t (20 ms in these simulations). The velocity row vector is multiplied by the head direction transformation matrix (H) to obtain the speed-modulated head direction vector $\vec{h}(t)$:

$$\bar{h} = \bar{v}(t)H = \bar{v}(t)\begin{bmatrix} \cos(\phi_1) & \cos(\phi_2) & \cos(\phi_3) & \cdots \\ \sin(\phi_1) & \sin(\phi_2) & \sin(\phi_3) & \end{bmatrix} \quad (5)$$

The model performs similarly with two different versions of speed-modulated head direction input, as used in the Burgess grid cell model

(Burgess *et al.*, 2007; Hasselmo *et al.*, 2007). As presented above, Eqn 5 produces head direction activity going positive and negative, and the grid cell model in Eqns 1 and 2 functions effectively with this input. However, because head direction cells have low background firing and increase their firing in only one direction, the model was also tested with the head direction vector rectified by a threshold linear function (with threshold zero). With this input, the grid cell model was modified to allow interactions of head direction inputs with differences of 180° (Burgess *et al.*, 2007; Hasselmo *et al.*, 2007).

In the matrix H, each value ϕ_i represents the preferred angle of one individual head direction cell. In most simulations, the preferred angles were set at intervals of $\pi/3$ radians (60°) and six head direction cells were used. As the velocity vector changes over time, $\vec{v}(t)$, this changes the speed-modulated head direction vector over time, $\vec{h}(t)$. The activity of speed-modulated head direction cells in the model is shown in Fig. 5. The tuning of two different cells to head direction is shown in Fig. 5A. The lines in Fig. 5B show the head direction vectors coded by the full population of head direction cells during waking (at every fifth time step for clarity). Here the vectors change systematically with the tangent of the trajectory. The lines in Fig. 5C show the head direction vector at every time point during REM replay.

Phases of grid cell oscillations code continuous location

The depolarization of grid cell dendrites by speed-modulated head direction input increases dendritic frequency and advances the phase of the dendritic oscillations in the grid cell model. This causes the change in phase of grid cell dendritic oscillations $\vec{\varphi}(t)$ to effectively integrate the speed-modulated head direction vector $\vec{h}(t)$, which is proportional to the velocity vector. This means that the two-dimensional spatial location vector $\vec{x}(t) = [x(t), y(t)]$ during waking is directly coded by the phase vector of grid cell dendritic oscillations (Hasselmo, 2007; Hasselmo *et al.*, 2007). The dendritic oscillation phase is scaled by the orientation selectivity of the head direction cells (represented by a matrix H) as well as the intrinsic frequency f of the grid cell, and the scaling factor B. The grid cell phase is related to the location vector $\vec{x}(t)$ at each time point relative to the starting location x_0 as follows: $\vec{\varphi}(t) - \varphi_k = (\vec{x}(t) - \vec{x}_0)H2\pi fB$. Therefore, the coding of two-dimensional location (relative to starting location) by dendritic oscillation phase can be obtained by using the inverse equation:

$$\vec{x}(t) - \vec{x}_0 = (\vec{\varphi}(t) - \varphi_k)H^{-1}/2\pi fB \qquad (6)$$

The internal representation of location can be obtained from the phase of just two grid cell dendrites by using the following inverse matrix (Strang, 1988) based on the head direction transform matrix in Eqn 5:

$$H^{-1} = \begin{bmatrix} \sin\phi_2 & -\sin \\ \cos\phi_2 & \cos\phi_1 \end{bmatrix} / (\cos\phi_1 \sin\phi_2 - \sin\phi_1 \cos\phi_2) \qquad (7)$$

Note that when the rectified version of the transform matrix is used, this requires combining phases before the transform in the same manner that head direction inputs were combined. The inverse transform of grid cell phase is used in Figs 6, 8, 9 and 12 to demonstrate how the activity of grid cells in the model codes continuous spatial location over time during waking, and how the phase of the same grid cells shifts in a systematic way due to temporally structured replay of trajectories during simulated REM sleep. In short, the inverse transform of grid cell phase allows continuous plotting of the internal representation of location during REM replay.

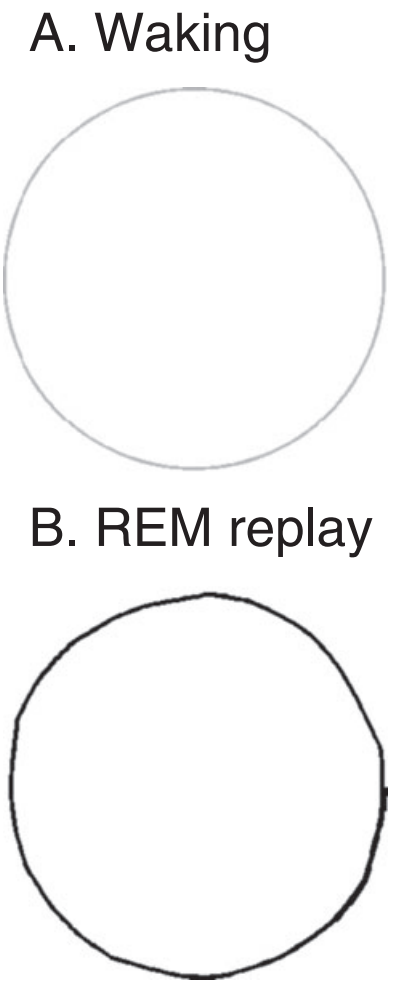

FIG. 6. The internal retrieval of trajectory during REM sleep matches the trajectory experienced during waking. (A) The circular trajectory experienced and encoded during waking behaviour (95 cm in diameter). (B) The inverse transform of the phase of entorhinal grid cell oscillations during REM sleep shows that internal retrieval effectively replicates the original trajectory. The retrieval (black) covers the plot of the waking trajectory (gray).

The integration of velocity by phase is sensitive to the accumulation of noise. Some simulations of encoding used random changes in running speed to test noise sensitivity, but the integration of velocity was assumed to be accurate to reduce the complexity of the simulation. Integration noise would require updating of phase by sensory input from the environment, as addressed in previous studies (Burgess *et al.*, 2007; Franzius *et al.*, 2007a).

Encoding during waking

Simulations of waking behavior focus on the rat moving in a circular trajectory over a period of 24 s (1200 steps). The movement for each 20-ms time step along this trajectory allows computation of the velocity vector that determines the activity of the head direction vector $\vec{h}(t)$ as shown in Eqn 5. During waking, the head direction activity is driven by sensory and proprioceptive input via the head direction circuit from brainstem structures through anterior thalamus to the postsubiculum (Goodridge & Taube, 1997; Sharp *et al.*, 2001; Taube & Bassett, 2003). The influence of feedback from hippocampal

place cells is modeled as weaker than the influence of excitatory sensory input that dominates head direction activity during waking (possibly due to feedforward inhibition). Neuromodulators could contribute to this difference in dynamics between waking and REM sleep (Hasselmo, 1999). The head direction vector updates the activity of grid cells according to Eqn 2. As the virtual rat moves, the grid cell activity shifts and causes sequential activation of different place cells via synaptic connections according to Eqn 4.

Encoding of the behavior during waking results from synaptic modification of the connections W_{PH} between the full population of place cells $\vec{p}(t)$ and the population of head direction cells $\vec{h}(t)$, as follows:

$$W_{PH}(t+1) = (W_{PH}(t) + \sum_t \vec{p}(t)^T \vec{h}(t))/2 \quad (8)$$

This equation updates the weights by the average of the previous weight and the outer product of the current place cell $\vec{p}(t)$ and head direction vector $\vec{h}(t)$. This synaptic modification provides the mechanism for later retrieval of movements associated with each place along the trajectory, but does not influence head direction activity during waking. Because the equation for synaptic modification depresses some connections while enhancing others, the initial pattern of connectivity has little effect. Most simulations started with W_{PH} as a matrix of zeros, but similar performance occurred during testing of a wide range of starting values. This matrix could correspond to direct projections from region CA1 of the hippocampus to the postsubiculum (van Groen & Wyss, 1990), or to the effect of projections from hippocampus to subiculum (Swanson *et al.*, 1978; Amaral & Witter, 1989), and projections from the subiculum to the postsubiculum and medial entorhinal cortex (Naber & Witter, 1998).

Temporally structured replay during REM sleep

During simulation of REM sleep, the network receives no direct sensory input. The network is only presented the initial pattern of grid cell, place cell and head direction activity on the first step that starts the replay. After this initial cue, the activity of head direction cells is determined entirely by the spread of activity across previously modified synapses W_{PH} from the hippocampus. For each new pattern of place cell activation, activity spreads across the connections W_{PH} to activate the associated head direction vector. The spread of activity from place cells to head direction cells is summarized by the following equation, which includes normalization based on the sum of all place cell activity.

$$\vec{h}(t) = \vec{p}(t) W_{PH} / \sum \vec{p}(t) \quad (9)$$

During REM replay, this head direction vector then causes a progressive shift in the phase of grid cell oscillations (Eqn 2) and a shift in the pattern of grid cell firing until spiking is induced in a new set of place cells (Eqn 4). If the transition to new place cell input is slow, the head direction vector is maintained by graded persistent firing of the head direction cells. Graded persistent firing has been shown in intracellular recording from neurons in deep layers of entorhinal cortex slice preparations (Egorov *et al.*, 2002; Fransén *et al.*, 2006) and persistent firing has been shown with whole cell patch recording in slices of postsubiculum (Yoshida & Hasselmo, 2008). These data on persistent spiking were observed in the presence of cholinergic agonists, indicating that these effects would be present during the high levels of acetylcholine present in cortical structures during REM sleep (Marrosu *et al.*, 1995). Thus, if necessary, the persistent firing allows head direction activity to continue for a period of time during which it causes a shift in frequency of oscillations in entorhinal grid cells.

The head direction vector causes a progressive shift in the phase of grid cell oscillations and a shift in the pattern of grid cell firing until spiking is induced in a new set of place cells. The new place cell activity then induces a new pattern of head direction firing $\vec{h}(t)$ according to Eqn 9 that further updates the pattern of grid cell activity, and the cycle of temporally structured replay continues. Thus, continuous REM replay depends upon interactions in a loop including connections from place cells $\vec{p}(t)$ to head direction cells $\vec{h}(t)$, from head direction cells $\vec{h}(t)$ to grid cells $\vec{g}(t)$, and from grid cells back to place cells $\vec{p}(t)$.

Results

In these simulations, interacting populations of grid cells, place cells and head direction cells encode the circular trajectory through the environment experienced during waking, and demonstrate temporally structured replay of the activity during simulated REM sleep, as summarized in Figs 5–12.

The temporally structured replay depends upon the spatial pattern of activity of different populations that are shown in Figs 2–5. The spiking activity that occurs in the population of grid cells in the model is shown during running in an open field environment in Fig. 2. The pattern of spiking activity in this population of grid cells effectively replicates the firing properties of grid cells recorded in medial entorhinal cortex during random foraging in an open field (Hafting *et al.*, 2005; Sargolini *et al.*, 2006; Fyhn *et al.*, 2007). The properties of the different grid cells shown in Fig. 2 are influenced by the oscillatory phase φ_{ik} that determines the spatial phase of grid cell firing in two dimensions, and by the parameter of baseline oscillation frequency f_j that determines the size and spacing of firing fields.

Figure 3 shows the pattern of firing of these grid cells during running on the circular track that is the primary focus of these simulations. Note that each grid cell shows multiple different firing fields on the circular track. The grid cell firing results from progressive input from head direction cells firing in response to progressively different head directions at different positions around the circle, as shown in Fig. 5B.

Individual cells in the population of place cells in the model replicate the highly localized firing fields of hippocampal place cells, as shown in Fig. 4 for an open field trajectory (Fig. 4A) and the circular track (Fig. 4B). The patterns of grid cell firing spread across the modified synapses W_{GP} from grid cells to place cells. The mechanism for initial selection of place cells results in connectivity from groups of grid cells with overlapping firing locations that results in the individual examples of localized place cell firing shown in Fig. 4A and B. The full set of 400 place cells effectively codes locations around most of the circular track, as shown by the plot in Fig. 4C showing spiking activity of all place cells in the population.

Individual head direction cells in the model respond when the rat moves in directions close to the preferred direction of the cell, as shown in Fig. 5A. These tuning curves resemble the data on cells with relatively wide tuning to head direction (Sharp, 1996; Sargolini *et al.*, 2006). During running on the circular track in the waking period, the head direction vector shows a progressive change in firing driven by the different head directions of the virtual rat as it runs, as shown in Fig. 5B. During REM sleep, the head direction cell vector is driven by

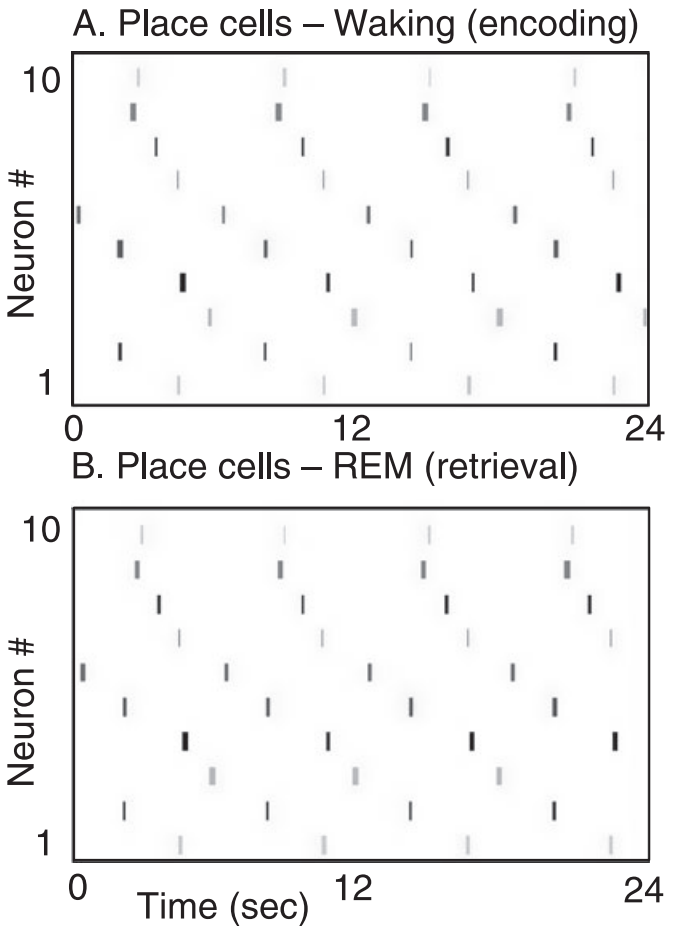

FIG. 7. Place cell activity during simulation of REM retrieval replicates the place cell activity during waking behavior. (A) Spiking activity of ten place cells during waking behavior. Spiking is shown in different rows during a period of 24 s of running the circular track, resulting in four full cycles of the track and four sequences of repeated spiking in the same place cells. (B) Spiking activity of the same ten place cells during simulated REM sleep (retrieval). Spiking is shown during a period of 24 s of simulated REM, during which the retrieval results in four full cycles of activation of the same sequence of place cells seen during waking.

the spread of activity across previously modified synapses W_{PH}. The retrieval mechanism causes progressive activation in the population of head direction cells that codes different directions of movement, as shown in Fig. 5C. During REM sleep, the retrieval mechanism does not run as smoothly as the input during waking, resulting in more variability in the direction and magnitude of the vectors representing head direction activity in Fig. 5C. However, this variability does not prevent effective retrieval function, and REM replay is similar even if noise is added to the head direction vectors during waking (encoding).

The progressive shift in activation of different head direction cells during the REM retrieval phase results in a systematic structured change in the phase of oscillations in simulated entorhinal grid cells, as shown in Fig. 6. The trajectory experienced during waking is shown in Fig. 6A. In Fig. 6B the inverse transform of the grid cell phase in Eqns 6 and 7 is used to plot the internal representation of location over time during REM sleep. As shown in Fig. 6B, the internal representation of location (black line) follows a trajectory through space that effectively matches the trajectory experienced during waking (Fig. 6A). There is some variation in the trajectory during different retrieval examples (see Fig. 8), but the network is usually able to retrieve the full trajectory effectively.

Most simulations set the initial conditions of replay to match the pattern of grid cell, place cell and head direction activity from the start of the waking encoding period. However, the network can perform replay with any initial conditions for head direction cells because the head direction activity during REM is determined by the synaptic input from place cells. In addition, the network can perform replay with any initial conditions for place cell activity because this activity is rapidly altered by the current grid cell input. Thus, the crucial initial conditions were determined by the grid cell phase. REM replay occurred for starting grid cell phases corresponding to locations experienced anywhere on the circular track. If the starting grid cell phase did not correspond to a location on the track, then the circuit of place cells and head direction cells was not activated, and the retrieval would drift randomly (unless it happened to overlap with a segment of the circular track).

Examples of the temporally structured replay of place cell activity during different simulations are shown in Figs 7 and 8. Individual simulations differ because of the random selection of grid to place connections. Figure 7 shows activity from one simulation in the form of ten place cells randomly selected from the full population of 400 place cells. The figure shows separate plots for place cell activity during simulated waking behavior (Fig. 7A) and during simulated REM sleep (Fig. 7B). During the 24-s simulated waking period, the pattern of place cell spiking activity is determined by the trajectory of actual movement through the environment. The virtual rat goes around the circular track four times, resulting in four cycles of sequential activation in the same set of ten place cells. During simulated REM sleep, the network starts with place cell activity in one location and this triggers four cycles of retrieval of the full circular trajectory. Due to the internal spread of retrieval activity, the network shows sequential place cell activity with spike timing similar to waking.

Figure 8 shows place cell activity during waking behavior and during simulated REM sleep for ten different simulations run separately with creation of different connectivity between grid cells and place cells for each simulation. Each row of the figure shows activity for a different simulation. Each box in column A shows spiking of ten place cells during waking, and the box in the same row of column B shows spiking of the same ten place cells during REM. Column C shows the inverse transform of grid cell phase indicating internal representation of location. In six out of ten cases, the pattern of place cell spiking during the full duration of REM replay closely resembles the pattern of spiking during waking. In these cases, the pattern of place cell spiking during REM shows the same temporal structure as the pattern of place cell spiking during waking.

In some cases, REM replay does not complete multiple cycles. This is consistent with the fact that replay is variable in experimental data. For instance, in the examples in rows 3 and 7, REM replay breaks down after one cycle of successful retrieval. This is also visible in the trajectory plots in rows 3 and 7 of column C. In Row 6, REM replay completes three cycles but then ceases. In Row 4, the internal representation during REM replay does not follow the circular track perfectly but still completes all cycles, activating a subset of the place cells activated during waking. In multiple groups of ten simulations, an average of six out of ten simulations showed successful completion of all cycles. The variation between different simulations results from the random selection of different place cells and the corresponding variation in distribution of synaptic weights between grid cells and place cells and between place cells and head direction cells. The consistency of retrieval could be enhanced by various techniques: for

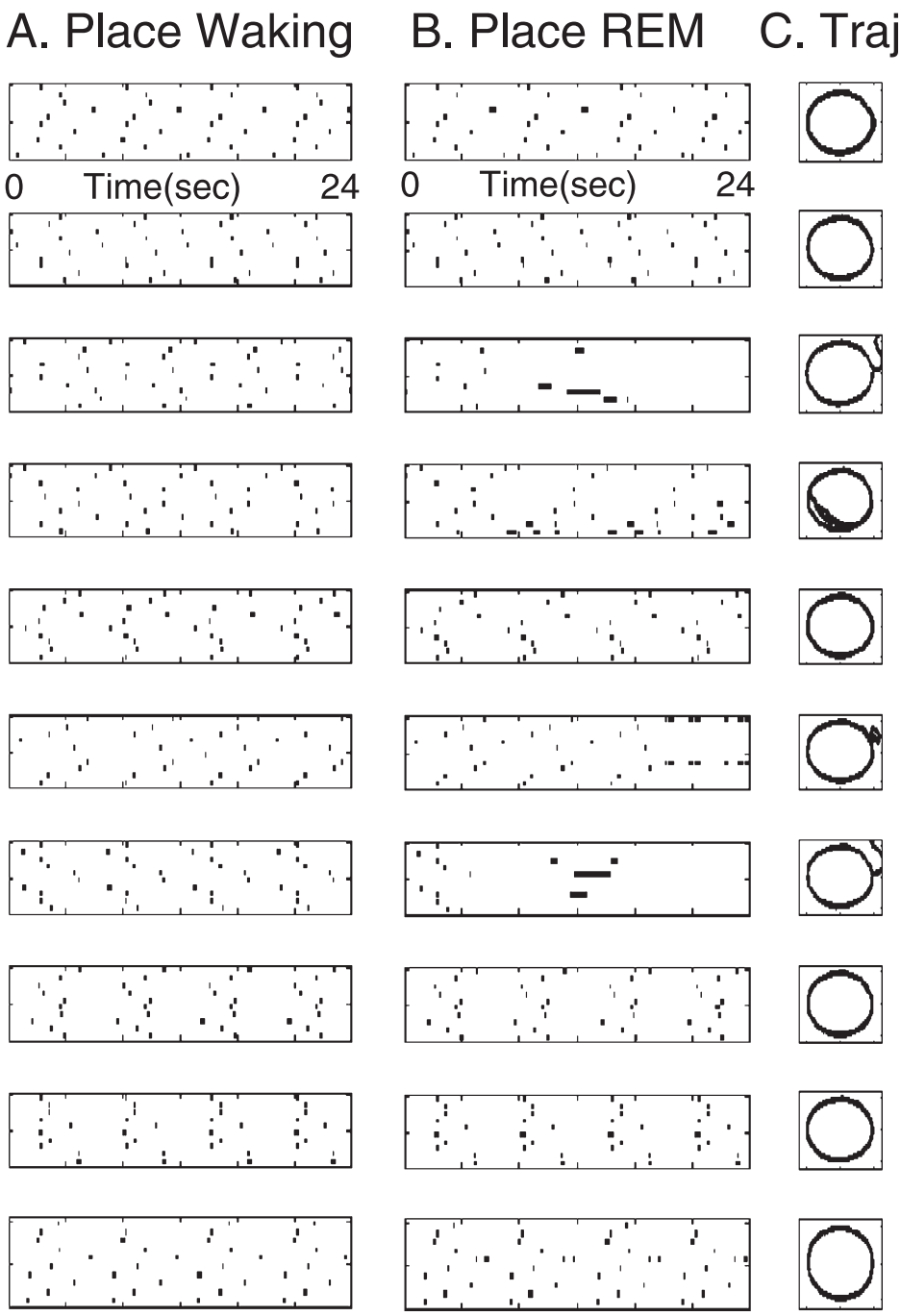

FIG. 8. Examples of place cell activity and retrieved trajectory during 10 different simulations of the full model. Each row shows a separate simulation. Six out of 10 simulations showed full replay during REM. Column A plots show spiking activity of 10 place cells during waking. Column B plots in the same row show spiking activity of the same ten place cells during REM replay. Note similarity of patterns in Column B to Column A. Column C plots the inverse transform of grid cell activity during REM, showing successful retrieval of the circular trajectory in six out of 10 cases (track diameter 95 cm). In unsuccessful cases, the trajectory diverges from the circular track.

example, associating place with angular velocity, or including cells responding to arc length (Hasselmo, 2007). However, the experimental data also show variability, and the features of this model could be evaluated by comparing properties of variance in the model with properties of variance in future experimental data.

The speed of temporally structured replay of place cell activity depends upon the magnitude of persistent firing in the head direction cells during REM replay, which is determined by the strength of connections W_{PH} from place cells to head direction cells. This can be demonstrated by altering the strength of W_{PH} by multiplying the matrix with a constant s with different values, as shown in Figs 9 and 10. As shown in Fig. 9, multiplying with $s = 0.5$ results in replay that is half the speed of waking (two cycles are completed during REM replay rather than four). Multiplying with $s = 1.5$ results in replay that is 50% faster than waking (six cycles vs. four). Setting s close to zero greatly slows the sequential activity. The replay can be graded to a range of different speeds, as shown in Fig. 10. In these figures, simulations with multiple cycles of successful replay were chosen for

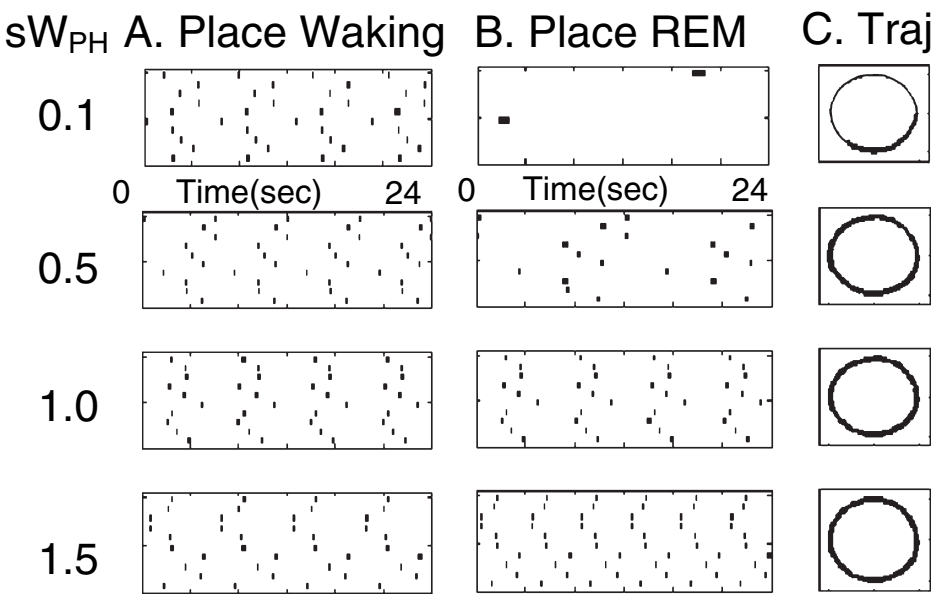

FIG. 9. Time course of REM replay determined by strength of connections from place cells to head direction cells W_{PH}. Column A shows place cell activity during waking, with same speed of movement. In each row of Column B, the connections W_{PH} are multiplied by a different value during REM replay. This results in different speeds of replay relative to waking, with s = 0.1 resulting in less than ½ cycle, s = 0.5 resulting in two cycles during 24 s, s = 1.0 resulting in four cycles, and s = 1.5 resulting in six cycles during 24 s. Thick black lines in column C show retrieved trajectories.

each value of s. Thus, the model predicts that faster replay corresponds to stronger synaptic connections from place cells to head direction cells, and higher firing rates in head direction cells. Previous studies have demonstrated how difficult it is to show learning-induced changes in synaptic strength (Moser *et al.*, 1993), but unit recording can test the prediction that higher head direction firing rates should be correlated with faster replay.

The temporal structure of replay can even account for changes in the movement speed of the rat during waking. As shown in Fig. 11, the simulation shows REM replay of a consistent change in running speed occurring near the reward location during waking. Figure 11A1, shows plots of the running speed (labelled 's') of the virtual rat in cm/s as well as one dimension of location (labelled 'x') in cm. In Fig. 11A1, the location x changes cyclically similar to a sine wave, as the rat runs around the circular track. Speed starts out as a straight line at 50 cm/s and then reduces to 5 cm/s near the reward location. In Fig. 11A2, there is no external influence on movement. The speed of movement is determined entirely by the spread of activity from place cells to head direction cells. In this case, REM replay still shows the same pattern as waking, with slowing of running speed to about 5 cm/s near reward location. Figure 11A4, shows that the pattern of place cell activity during REM replay matches that seen during waking (Fig. 11A3), with a longer period of place cell activity during slowing.

REM replay is not altered by noise added to the running speed, as shown in Fig. 11B. In this figure, random changes in running speed were added in proportion to 30% of total running speed. This does not prevent the REM replay in Fig. 11B2 from showing the same pattern of location and speed changes that appear during waking in Fig. 11B1. Performance was similar if speed was assumed to be uniform but noise was added at the stage of the speed-modulated head direction activity. Note that this example shows transient reduction of running speed to 25 cm/s during waking and REM replay, to illustrate the capacity to match different quantitative changes in running speed. Note that noise results in changes in running speed that are recapitulated during each cycle of REM replay. Figure 11C shows that the REM replay also replicates changes in the baseline running speed from 50 to 25 cm/s (note the increase in simulation period to 48 s).

As noted above, the speed of REM replay depends upon the magnitude of synaptic transmission on the synapses W_{PH} from place cells to head direction cells. Systematic changes in strength due to a multiplier of W_{PH} cause systematic changes in number of cycles during replay, as shown in Fig. 12A. The success of retrieval also depends upon the number of place cells used in the network, as shown in Fig. 12B. This figure shows the average number of cycles of REM replay for ten simulations run with different numbers of place cells (and with noise set at 20%). The waking period was 24 s, but each simulation was tested for the number of cycles during a longer period of 48 s of REM replay. For small numbers of place cells (e.g. between 36 and 256 place cells), there was less than one cycle of REM replay in the majority of cases, and the mean number of cycles completed was fewer than two. In contrast, for larger numbers of place cells (e.g. 324 and higher), the average number of cycles of REM replay jumps up to over three, indicating successful REM replay of multiple cycles in most simulations. This shows that when a sufficient number of place cells provide a high-resolution representation of place in the environment, the network performs successful REM replay of multiple cycles of the task.

These simulations propose a potential mechanism for REM replay in place cells, and generate predictions that REM replay should appear in other populations of cells, including both head direction cells and grid cells, with specific timing in coordination with the place cell activity. As shown in Fig. 12C, this model predicts that entorhinal grid cells should show patterns of activity during REM sleep that correlate with the patterns of activity present during waking behaviour. Figure 12C5 shows that the pattern of grid cell activity during simulated REM closely resembles the pattern of grid cell activity induced by running on the circular track during waking, as shown in Fig. 12C4. Thus, these simulations generate detailed predictions about the expected pattern of spiking activity during REM replay.

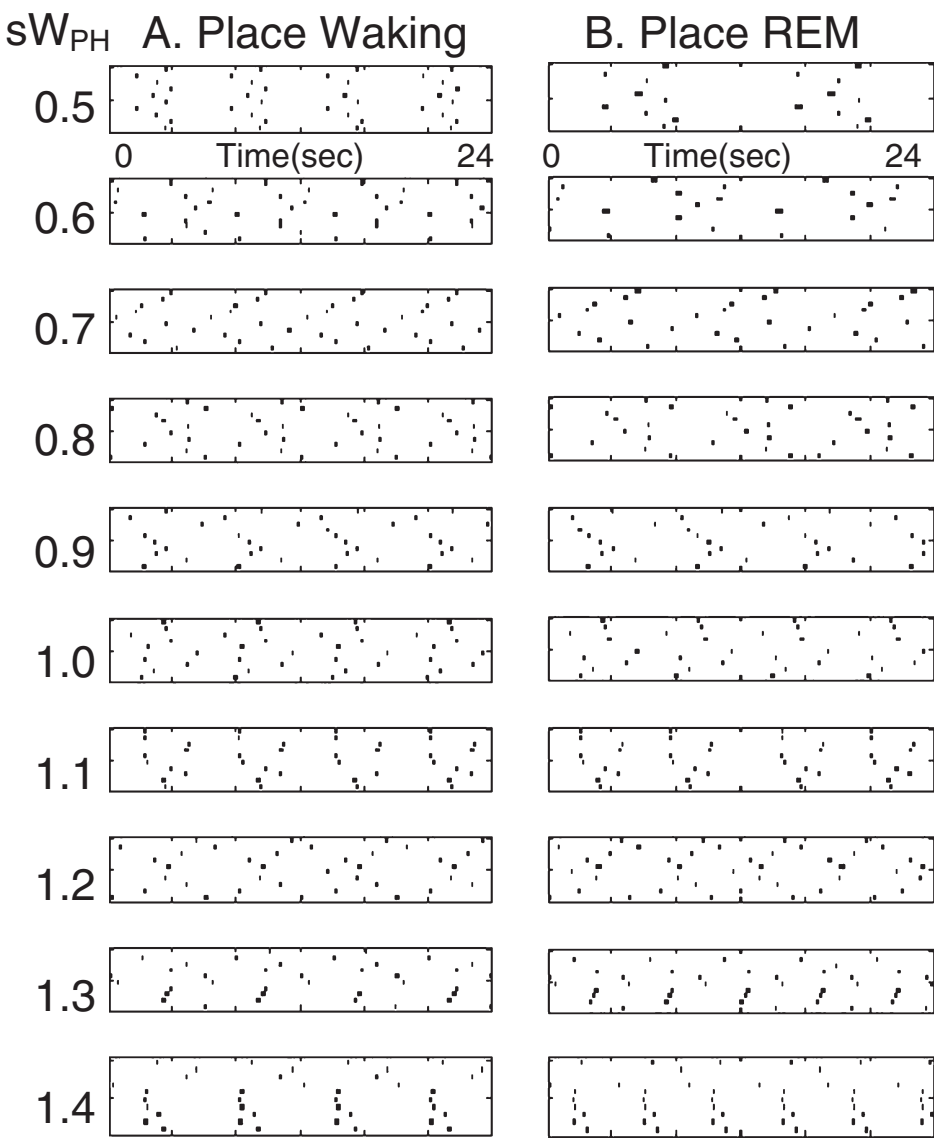

FIG. 10. Ten examples of REM replay with different strengths of connections from place cells to head direction cells W_{PH}. Column A shows place cell activity during waking, with same speed of movement. In each row of Column B, the connections W_{PH} are multiplied by a different value (shown on left) during REM replay. This results in different speeds of replay relative to waking.

Discussion

The simulations presented here show how temporally structured replay during REM sleep (Louie & Wilson, 2001) could arise from a circuit including grid cells, place cells and head direction cells. Place cells in the simulation respond to the circular trajectory during waking (Figs 7A and 8A), and the same place cells are activated sequentially in the absence of sensory input during the simulation of REM replay (Figs 7B and 8B). The sequential readout of place cell activity during simulated REM sleep matches the timing of place cell activity during waking, including changes in the speed of movement (Fig. 11). The inverse transform of grid cell phase shows that the internal representation of the trajectory during simulated REM sleep closely matches the trajectory experienced during waking (Figs 6, 8 and 9).

These simulations demonstrate a potential mechanism for the temporally structured replay of place cell activity during REM sleep demonstrated experimentally using multiple single unit recording in rats (Louie & Wilson, 2001). Similar to the data, the simulation shows REM replay with temporal scaling similar to waking activity. Changes in the strength of synaptic connections between place cells and head direction cells (Figs 9 and 10) alter the speed of REM replay relative to waking in a manner that resembles the variability in scaling factor seen in the data for different REM episodes (Louie & Wilson, 2001).

The model presented here generates the prediction that head direction activity should show a corresponding replay of sequences occurring during waking. This prediction of the model motivated experiments that show head direction cell activity during REM sleep that correlates with prior waking behavior (Brandon *et al.*, 2008). The model also generates the prediction that grid cell activity in entorhinal cortex should show replay of particular sequences occurring during waking (Fig. 12).

This model could function with any of a wide range of different grid cell models (Fuhs & Touretzky, 2006; McNaughton *et al.*, 2006; Blair *et al.*, 2007; Burgess *et al.*, 2007), as long as they perform path integration based on head direction and speed. The simulations shown here used grid cell activity based on a previously published model of

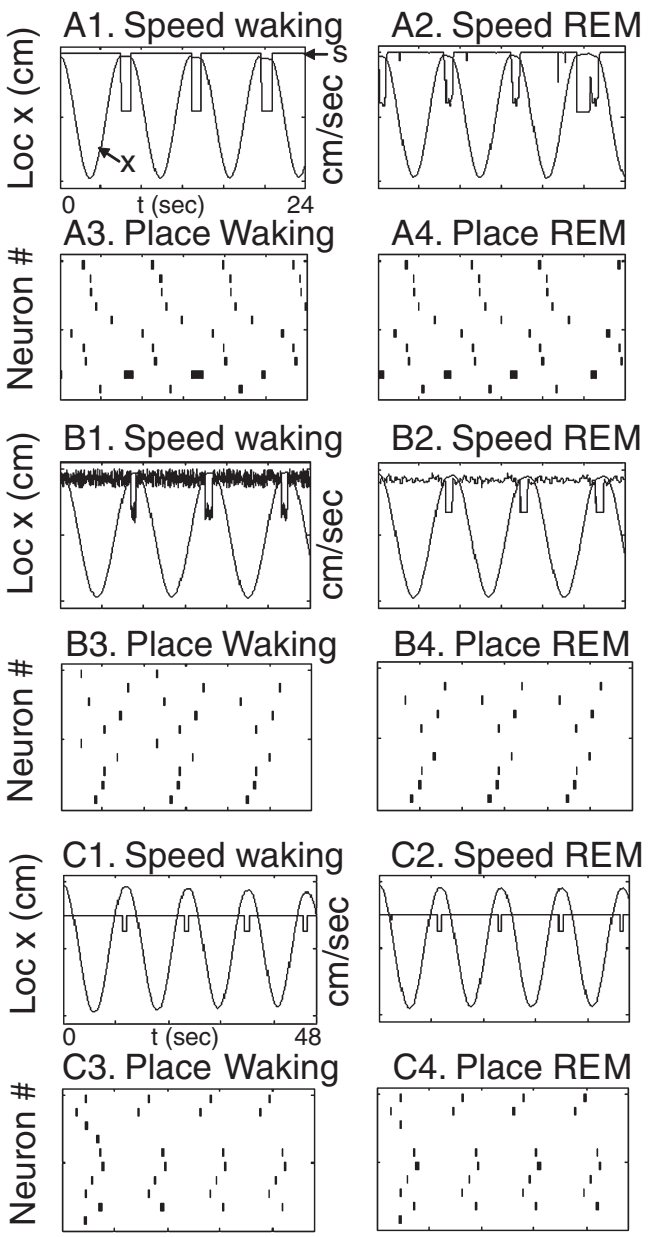

FIG. 11. REM replay can replicate changes in running speed during waking. (A1) During waking, location (in cm) changes cyclically as rat traverses circular track (line marked x). Top line on same plot shows speed in cm/s (line marked s), starting with a steady speed of 50 cm/s, and reducing to 5 cm/s during each approach to the reward location (when x approaches 50 cm). (A2) REM replay shows the same slowing of speed near the reward location. (A3) Place cell firing during waking shows extended place cell activity near reward location that also occurs during REM replay (A4). (B1) Network performance is similar with addition of noise to the movement speed during waking. To show the capacity to replicate different speed changes, the external change in speed goes from 50 to 25 cm/s near reward location. (B2) REM replay shows similar changes in speed (note similar pattern of noise on each cycle). (B3) Place cell activity during waking resembles place cell activity during REM replay (B4). (C1) The network performance is similar when movement starts at 25 cm/s and reduces to 12.5 cm/s near reward. (C2) REM replay shows similar changes in speed, and place cell activity during waking (C3) resembles that during REM replay (C4). Note that plots show 24 s in A and B and 48 s in C.

medial entorhinal grid cells (Burgess *et al.*, 2005, 2007; O'Keefe & Burgess, 2005) based on earlier models of theta phase precession (O'Keefe & Recce, 1993; Lengyel *et al.*, 2003). In this model, input from different head direction cells to single entorhinal grid cells alters the frequency and phase of dendritic oscillations relative to each other, resulting in an interference pattern that replicates grid cell firing (Burgess *et al.*, 2007; Hasselmo *et al.*, 2007). As shown in Figs 2 and 3, the model produces grid cells with different properties of field spacing and size that depend upon the baseline oscillation frequency within each neuron. The grid cell firing corresponds to differences in field spacing and size seen along the dorsal to ventral axis of medial entorhinal cortex (Hafting *et al.*, 2005; Sargolini *et al.*, 2006; Fyhn *et al.*, 2007), and the oscillation frequency difference corresponds to the experimental data showing membrane potential oscillation differences along the dorsal to ventral axis of medial entorhinal cortex (Giocomo *et al.*, 2007; Hasselmo *et al.*, 2007). The same circuit presented here could function with other models of grid cells, including models using network attractor dynamics updated by head direction input (Fuhs & Touretzky, 2006; McNaughton *et al.*, 2006). This grid cell model is mathematically similar to a grid cell model created using the mechanism of persistent firing (Hasselmo, 2008; Hasselmo & Brandon, 2008) in which grid cell firing arises from convergent input from persistent spiking neurons with specific phase relationships determined by head direction.

The simulation presented here could function with a range of mechanisms for creating place cells from grid cell input (Fuhs & Touretzky, 2006; McNaughton *et al.*, 2006; Rolls *et al.*, 2006; Solstad *et al.*, 2006; Franzius *et al.*, 2007b; Molter & Yamaguchi, 2007). The mechanism presented here selects place cells with spatial variance below a chosen value and strengthens synaptic input to these place cells from medial entorhinal grid cells. The size of place cell firing fields necessary for effective function in the model is consistent with evidence for the size of place cell firing fields in the hippocampus.

The most specific requirements of the model presented here concern the nature of head direction responses and the influence of place cells on head direction cells. Extensive experimental data describe head direction cells in areas receiving output from the hippocampal formation, including the deep layers of the entorhinal cortex (Sargolini *et al.*, 2006) and the postsubiculum (dorsal presubiculum) (Taube *et al.*, 1990a, 1996; Knierim *et al.*, 1995; Taube & Burton, 1995; Sharp, 1996; Sharp *et al.*, 2001; Taube & Bassett, 2003). The influence of place cells on head direction cells could underlie data showing cells with a combination of place and head direction dependence in the presubiculum and parasubiculum (Cacucci *et al.*, 2004). The head direction tuning width used here matches data on cells with relatively wide head direction tuning (Sharp, 1996; Sargolini *et al.*, 2006), but narrower tuning could be used with a different grid cell model. The current simulation uses head direction activity modulated by movement speed. Some neurons show speed modulation in deep entorhinal cortex (Sargolini *et al.*, 2006), postsubiculum (Taube *et al.*, 1990b; Sharp, 1996) and related structures (O'Keefe *et al.*, 1998; Sharp & Turner-Williams, 2005; Sharp *et al.*, 2006). However, this aspect of the circuit might require activation of separate populations of cells that then converge on the grid cell representation.

Because head direction cells are also seen in retrospenial cortex (Cho & Sharp, 2001), the reactivation of head direction cells during retrieval could underlie evidence for activation of retrosplenial cortex in humans during performance of autobiographical memory tasks (Piefke *et al.*, 2003; Steinvorth *et al.*, 2006) and spatial memory tasks (Epstein *et al.*, 2007; Iaria *et al.*, 2007).

The oscillatory dynamics used in the grid cell model are consistent with the theta frequency field potential oscillations that appear prominently in layers of the hippocampus where synaptic input arrives from the entorhinal cortex (Brankack *et al.*, 1993; Booth & Poe, 2006; Hasselmo *et al.*, 2007), and with differences in intrinsic frequency of

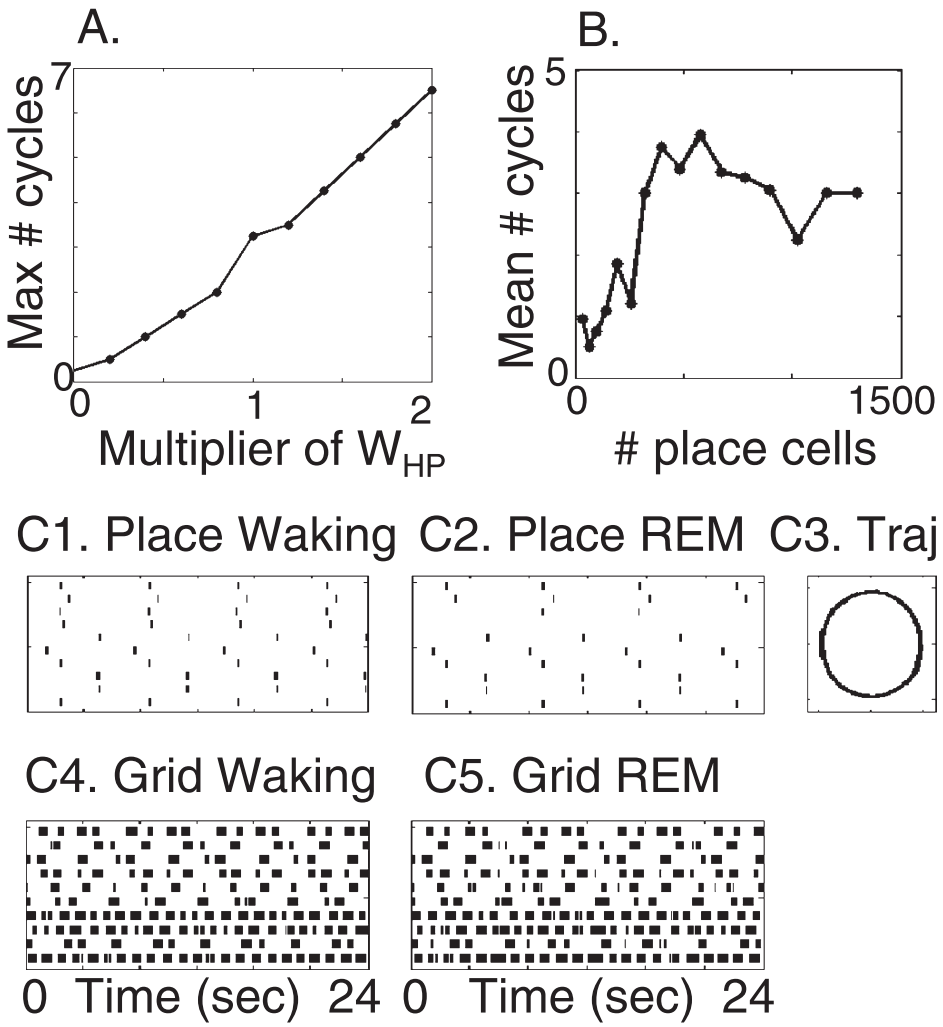

FIG. 12. Number of cycles of successful REM replay with changes in different parameters. (A) The number of cycles of REM replay increases in proportion to the multiplier of W_{PH}. (B) The number of cycles of successful REM replay depends upon total number of place cells, with good performance starting at 324 cells and remaining high for larger numbers. (C) This model simulating place cell activity during waking (C1) and REM sleep (C2) generates the prediction that grid cell activity during REM sleep (C5) should correlate with grid cell activity associated with running the circular track during waking (C4). (C3) Shows trajectory retrieval.

neurons along the dorsal to ventral axis of the hippocampus (Maurer *et al.*, 2005).

If the same location in the environment is associated with multiple different head directions or speeds, this can cause ambiguity for replay. This ambiguity can be overcome by neural activity dependent upon the trajectory arc length or temporal duration from a recent stopping point. Arc length coding can be obtained in the model by resetting oscillatory phase at stopping locations (Hasselmo, 2007, 2008) and removing the influence of head direction by using input from cells modulated by speed alone (Sharp, 1996; O'Keefe *et al.*, 1998; Sharp *et al.*, 2006). The simulation of arc-length coding (Hasselmo, 2007) closely matches spiking properties of hippocampal neurons that respond selectively dependent on recent context in tasks such as spatial alternation (Lee *et al.*, 2006) and delayed non-match to position (Griffin *et al.*, 2007).

If the influence of external sensory input is reduced for a period during waking, the circuit presented here could perform episodic retrieval of previously experienced trajectories during waking. This could underlie data on forward replay of place cell activity corresponding to experienced trajectories shown experimentally during waking behavior (Foster & Wilson, 2006; Diba & Buzsaki, 2007; Johnson & Redish, 2007). The model does not address reverse replay of sequences, but this reverse replay has not been demonstrated during REM sleep replay (Louie & Wilson, 2001). With appropriate increases in replay speed, this circuit could also underlie forward hippocampal replay occurring during slow wave sleep (Skaggs & McNaughton, 1996; Nadasdy *et al.*, 1999) that could drive the replay shown in neocortical structures (Ribeiro *et al.*, 2004; Euston *et al.*, 2007; Ji & Wilson, 2007). However, the faster time scale of replay in these other studies would require a stronger influence of place cells on head direction cells, or an increase in oscillation frequencies in entorhinal cortex. Faster replay could also be due to direct associations between place cells coding states, rather than the slower mechanisms of state to action association used here for temporally structured replay.

The sequence replay mechanisms simulated here could prove important both for consolidation of trajectories in the environment and for episodic retrieval of trajectories. Experimental data support an important role of the hippocampus in learning the sequential order of events or stimuli in the environment (Eichenbaum *et al.*, 1999). This could involve association of elements of a trajectory with individual events or stimuli. Lesions of the hippocampus impair the ability to

learn and disambiguate non-spatial sequences such as a sequence of odors in a sequential discrimination task (Agster *et al.*, 2002) and impair the ability to retrieve information about the order of stimuli (Fortin *et al.*, 2002; Kesner *et al.*, 2002). In addition, lesions of the hippocampus impair performance in spatial tasks requiring memory for the previous spatial trajectory performed within a task (Ennaceur *et al.*, 1996; Ainge *et al.*, 2007). Performance in tasks requiring memory for spatial trajectories is also impaired by lesions of the entorhinal cortex (Steffenach *et al.*, 2005) and the postsubiculum (Taube *et al.*, 1992; Calton *et al.*, 2003), indicating the importance of the other components of the circuit simulated in this paper. The impairments caused by these lesions could be related to loss of the ability to encode and retrieve temporally structured sequences of activity.

Acknowledgements

I appreciate comments on the text from Mark P. Brandon. This research was supported by Silvio O. Conte Center grants NIMH MH71702, NIMH R01 MH60013, NIMH R01 MH61492, NIMH MH60450, NSF SLC SBE 0354378 and NIDA R01 DA16454 (part of the CRCNS program).

Abbreviation

REM, rapid eye movement.

References

Agster, K.L., Fortin, N.J. & Eichenbaum, H. (2002) The hippocampus and disambiguation of overlapping sequences. *J. Neurosci.*, **22**, 5760–5768.

Ainge, J.A., van der Meer, M.A., Langston, R.F. & Wood, E.R. (2007) Exploring the role of context-dependent hippocampal activity in spatial alternation behavior. *Hippocampus*, **17**, 988–1002.

Alonso, A. & Klink, R. (1993) Differential electroresponsiveness of stellate and pyramidal-like cells of medial entorhinal cortex layer II. *J. Neurophysiol.*, **70**, 128–143.

Alonso, A. & Llinas, R.R. (1989) Subthreshold Na-dependent theta-like rhythmicity in stellate cells of entorhinal cortex layer II. *Nature*, **342**, 175–177.

Amaral, D.G. & Witter, M.P. (1989) The 3-dimensional organization of the hippocampal formation – a review of anatomical data. *Neuroscience*, **31**, 571–591.

Blair, H.T., Welday, A.C. & Zhang, K. (2007) Scale-invariant memory representations emerge from moire interference between grid fields that produce theta oscillations: a computational model. *J. Neurosci.*, **27**, 3211–3229.

Booth, V. & Poe, G.R. (2006) Input source and strength influences overall firing phase of model hippocampal CA1 pyramidal cells during theta: relevance to REM sleep reactivation and memory consolidation. *Hippocampus*, **16**, 161–173.

Brandon, M.P., Andrews, C.M. & Hasselmo, M.E. (2008) Postsubicular neural activity during REM sleep shows replay of head direction activity during waking. *Abstr. Soc. Neurosci.*, **34**, 94.14.

Brankack, J., Stewart, M. & Fox, S.E. (1993) Current source density analysis of the hippocampal theta rhythm: associated sustained potentials and candidate synaptic generators. *Brain Res.*, **615**, 310–327.

Burgess, N., Barry, C., Jeffery, K.J. & O'Keefe, J. (2005) A grid and place cell model of path integration utilizing phase precession versus theta. In O'Reilly, R.C. & Glanzman, D. (Eds), *Computational Cognitive Neuroscience Meeting*. Nov. 10–11, 2005, Washington, D.C., pp. IV–2.

Burgess, N., Barry, C. & O'Keefe, J. (2007) An oscillatory interference model of grid cell firing. *Hippocampus*, **17**, 801–812.

Caballero-Bleda, M. & Witter, M.P. (1993) Regional and laminar organization of projections from the presubiculum and parasubiculum to the entorhinal cortex: an anterograde tracing study in the rat. *J. Comp. Neurol.*, **328**, 115–129.

Cacucci, F., Lever, C., Wills, T.J., Burgess, N. & O'Keefe, J. (2004) Theta-modulated place-by-direction cells in the hippocampal formation in the rat. *J. Neurosci.*, **24**, 8265–8277.

Calton, J.L., Stackman, R.W., Goodridge, J.P., Archey, W.B., Dudchenko, P.A. & Taube, J.S. (2003) Hippocampal place cell instability after lesions of the head direction cell network. *J. Neurosci.*, **23**, 9719–9731.

Cho, J. & Sharp, P.E. (2001) Head direction, place, and movement correlates for cells in the rat retrosplenial cortex. *Behav. Neurosci.*, **115**, 3–25.

Diba, K. & Buzsaki, G. (2007) Forward and reverse hippocampal place-cell sequences during ripples. *Nat. Neurosci.*, **10**, 1241–1242.

Dickson, C.T., Magistretti, J., Shalinsky, M.H., Fransen, E., Hasselmo, M.E. & Alonso, A. (2000) Properties and role of I(h) in the pacing of subthreshold oscillations in entorhinal cortex layer II neurons. *J. Neurophysiol.*, **83**, 2562–2579.

Egorov, A.V., Hamam, B.N., Fransen, E., Hasselmo, M.E. & Alonso, A.A. (2002) Graded persistent activity in entorhinal cortex neurons. *Nature*, **420**, 173–178.

Eichenbaum, H., Dudchenko, P., Wood, E., Shapiro, M. & Tanila, H. (1999) The hippocampus, memory, and place cells: is it spatial memory or a memory space? *Neuron*, **23**, 209–226.

Ennaceur, A., Neave, N. & Aggleton, J.P. (1996) Neurotoxic lesions of the perirhinal cortex do not mimic the behavioural effects of fornix transection in the rat. *Behav. Brain Res.*, **80**, 9–25.

Epstein, R.A., Parker, W.E. & Feiler, A.M. (2007) Where am I now? Distinct roles for parahippocampal and retrosplenial cortices in place recognition. *J. Neurosci.*, **27**, 6141–6149.

Euston, D.R., Tatsuno, M. & McNaughton, B.L. (2007) Fast-forward playback of recent memory sequences in prefrontal cortex during sleep. *Science*, **318**, 1147–1150.

Fortin, N.J., Agster, K.L. & Eichenbaum, H.B. (2002) Critical role of the hippocampus in memory for sequences of events. *Nat. Neurosci.*, **5**, 458–462.

Foster, D.J. & Wilson, M.A. (2006) Reverse replay of behavioural sequences in hippocampal place cells during the awake state. *Nature*, **440**, 680–683.

Fransén, E., Tahvildari, B., Egorov, A.V., Hasselmo, M.E. & Alonso, A.A. (2006) Mechanism of graded persistent cellular activity of entorhinal cortex layer v neurons. *Neuron*, **49**, 735–746.

Franzius, M., Sprekeler, H. & Wiskott, L. (2007a) Slowness and sparseness lead to place, head-direction, and spatial-view cells. *PLoS Comput. Biol.*, **3**, e166.

Franzius, M., Vollgraf, R. & Wiskott, L. (2007b) From grids to places. *J. Comput. Neurosci.*, **22**, 297–299.

Fuhs, M.C. & Touretzky, D.S. (2006) A spin glass model of path integration in rat medial entorhinal cortex. *J. Neurosci.*, **26**, 4266–4276.

Fyhn, M., Hafting, T., Treves, A., Moser, M.B. & Moser, E.I. (2007) Hippocampal remapping and grid realignment in entorhinal cortex. *Nature*, **446**, 190–194.

Giocomo, L.M., Zilli, E.A., Fransen, E. & Hasselmo, M.E. (2007) Temporal frequency of subthreshold oscillations scales with entorhinal grid cell field spacing. *Science*, **315**, 1719–1722.

Goodridge, J.P. & Taube, J.S. (1997) Interaction between the postsubiculum and anterior thalamus in the generation of head direction cell activity. *J. Neurosci.*, **17**, 9315–9330.

Griffin, A.L., Eichenbaum, H. & Hasselmo, M.E. (2007) Spatial representations of hippocampal CA1 neurons are modulated by behavioral context in a hippocampus-dependent memory task. *J. Neurosci.*, **27**, 2416–2423.

van Groen, T. & Wyss, J.M. (1990) The postsubicular cortex in the rat: characterization of the fourth region of the subicular cortex and its connections. *Brain Res.*, **529**, 165–177.

Hafting, T., Fyhn, M., Molden, S., Moser, M.B. & Moser, E.I. (2005) Microstructure of a spatial map in the entorhinal cortex. *Nature*, **436**, 801–806.

Hasselmo, M.E. (1999) Neuromodulation: acetylcholine and memory consolidation. *Trends Cogn. Sci.*, **3**, 351–359.

Hasselmo, M.E. (2007) Arc length coding by interference of theta frequency oscillations may underlie context-dependent hippocampal unit data and episodic memory function. *Learn Mem.*, **14**, 782–794.

Hasselmo, M.E. (2008) Grid cell mechanisms and function: contributions of entorhinal persistent spiking and phase resetting. *Hippocampus* in press.

Hasselmo, M.E. & Brandon, M.A. (2008) Linking cellular mechanisms to behaviour: entorhinal persistent spiking and membrane potential oscillations may underlie path integration, grid cell firing and episodic memory. *Neural Plast.*, **2008**, 658323.

Hasselmo, M.E. & Eichenbaum, H. (2005) Hippocampal mechanisms for the context-dependent retrieval of episodes. *Neural Netw.*, **18**, 1172–1190.

Hasselmo, M.E., Giocomo, L.M. & Zilli, E.A. (2007) Grid cell firing may arise from interference of theta frequency membrane potential oscillations in single neurons. *Hippocampus*, **17**, 1252–1271.

Iaria, G., Chen, J.K., Guariglia, C., Ptito, A. & Petrides, M. (2007) Retrosplenial and hippocampal brain regions in human navigation: complementary functional contributions to the formation and use of cognitive maps. *Eur. J. Neurosci.*, **25**, 890–899.

Jensen, O. & Lisman, J.E. (1996a) Hippocampal CA3 region predicts memory sequences: accounting for the phase precession of place cells. *Learn. Mem.*, **3**, 279–287.

Jensen, O. & Lisman, J.E. (1996b) Theta/gamma networks with slow NMDA channels learn sequences and encode episodic memory: role of NMDA channels in recall. *Learn. Mem.*, **3**, 264–278.

Ji, D. & Wilson, M.A. (2007) Coordinated memory replay in the visual cortex and hippocampus during sleep. *Nat. Neurosci.*, **10**, 100–107.

Johnson, A. & Redish, A.D. (2007) Neural ensembles in CA3 transiently encode paths forward of the animal at a decision point. *J. Neurosci.*, **27**, 12176–12189.

Kesner, R.P., Gilbert, P.E. & Barua, L.A. (2002) The role of the hippocampus in memory for the temporal order of a sequence of odors. *Behav. Neurosci.*, **116**, 286–290.

Knierim, J.J., Kudrimoti, H.S. & McNaughton, B.L. (1995) Place cells, head direction cells, and the learning of landmark stability. *J. Neurosci.*, **15**, 1648–1659.

Knierim, J.J., Kudrimoti, H.S. & McNaughton, B.L. (1998) Interactions between idiothetic cues and external landmarks in the control of place cells and head direction cells. *J. Neurophysiol.*, **80**, 425–446.

Lee, A.K. & Wilson, M.A. (2002) Memory of sequential experience in the hippocampus during slow wave sleep. *Neuron*, **36**, 1183–1194.

Lee, I., Rao, G. & Knierim, J.J. (2004a) A double dissociation between hippocampal subfields: differential time course of CA3 and CA1 place cells for processing changed environments. *Neuron*, **42**, 803–815.

Lee, I., Yoganarasimha, D., Rao, G. & Knierim, J.J. (2004b) Comparison of population coherence of place cells in hippocampal subfields CA1 and CA3. *Nature*, **430**, 456–459.

Lee, I., Griffin, A.L., Zilli, E.A., Eichenbaum, H. & Hasselmo, M.E. (2006) Gradual translocation of spatial correlates of neuronal firing in the hippocampus toward prospective reward locations. *Neuron*, **51**, 639–650.

Lengyel, M., Szatmary, Z. & Erdi, P. (2003) Dynamically detuned oscillations account for the coupled rate and temporal code of place cell firing. *Hippocampus*, **13**, 700–714.

Levy, W.B. (1996) A sequence predicting CA3 is a flexible associator that learns and uses context to solve hippocampal-like tasks. *Hippocampus*, **6**, 579–590.

Louie, K. & Wilson, M.A. (2001) Temporally structured replay of awake hippocampal ensemble activity during rapid eye movement sleep. *Neuron*, **29**, 145–156.

Marrosu, F., Portas, C., Mascia, M.S., Casu, M.A., Fa, M., Giagheddu, M., Imperato, A. & Gessa, G.L. (1995) Microdialysis measurement of cortical and hippocampal acetylcholine release during sleep-wake cycle in freely moving cats. *Brain Res.*, **671**, 329–332.

Maurer, A.P., Vanrhoads, S.R., Sutherland, G.R., Lipa, P. & McNaughton, B.L. (2005) Self-motion and the origin of differential spatial scaling along the septo-temporal axis of the hippocampus. *Hippocampus*, **15**, 841–852.

McNaughton, B.L., Battaglia, F.P., Jensen, O., Moser, E.I. & Moser, M.B. (2006) Path integration and the neural basis of the 'cognitive map'. *Nat. Rev. Neurosci.*, **7**, 663–678.

Molter, C. & Yamaguchi, Y. (2007) Impact of temporal coding of presynaptic entorhinal cortex grid cells on the formation of hippocampal place fields. *Neural Netw.*, **18**, 919–928.

Moser, E., Mathiesen, I. & Andersen, P. (1993) Association between brain temperature and dentate field potentials in exploring and swimming rats. *Science*, **259**, 1324–1326.

Naber, P.A. & Witter, M.P. (1998) Subicular efferents are organized mostly as parallel projections: a double-labeling, retrograde-tracing study in the rat. *J. Comp. Neurol.*, **393**, 284–297.

Nadasdy, Z., Hirase, H., Czurko, A., Csicsvari, J. & Buzsaki, G. (1999) Replay and time compression of recurring spike sequences in the hippocampus. *J. Neurosci.*, **19**, 9497–9507.

O'Keefe, J. (1976) Place units in the hippocampus of the freely moving rat. *Exp. Neurol.*, **51**, 78–109.

O'Keefe, J. & Burgess, N. (2005) Dual phase and rate coding in hippocampal place cells: theoretical significance and relationship to entorhinal grid cells. *Hippocampus*, **15**, 853–866.

O'Keefe, J. & Recce, M.L. (1993) Phase relationship between hippocampal place units and the EEG theta rhythm. *Hippocampus*, **3**, 317–330.

O'Keefe, J., Burgess, N., Donnett, J.G., Jeffery, K.J. & Maguire, E.A. (1998) Place cells, navigational accuracy, and the human hippocampus. *Philos. Trans. R. Soc. Lond. B Biol. Sci.*, **353**, 1333–1340.

Piefke, M., Weiss, P.H., Zilles, K., Markowitsch, H.J. & Fink, G.R. (2003) Differential remoteness and emotional tone modulate the neural correlates of autobiographical memory. *Brain*, **126**, 650–668.

Ribeiro, S., Gervasoni, D., Soares, E.S., Zhou, Y., Lin, S.C., Pantoja, J., Lavine, M. & Nicolelis, M.A. (2004) Long-lasting novelty-induced neuronal reverberation during slow-wave sleep in multiple forebrain areas. *PLoS Biol.*, **2**, E24.

Rolls, E.T., Stringer, S.M. & Elliot, T. (2006) Entorhinal cortex grid cells can map to hippocampal place cells by competitive learning. *Network*, **17**, 447–465.

Sargolini, F., Fyhn, M., Hafting, T., McNaughton, B.L., Witter, M.P., Moser, M.B. & Moser, E.I. (2006) Conjunctive representation of position, direction, and velocity in entorhinal cortex. *Science*, **312**, 758–762.

Sharp, P.E. (1996) Multiple spatial/behavioral correlates for cells in the rat postsubiculum: multiple regression analysis and comparison to other hippocampal areas. *Cereb. Cortex*, **6**, 238–259.

Sharp, P.E. & Turner-Williams, S. (2005) Movement-related correlates of single-cell activity in the medial mammillary nucleus of the rat during a pellet-chasing task. *J. Neurophysiol.*, **94**, 1920–1927.

Sharp, P.E., Blair, H.T. & Cho, J. (2001) The anatomical and computational basis of the rat head-direction cell signal. *Trends Neurosci.*, **24**, 289–294.

Sharp, P.E., Turner-Williams, S. & Tuttle, S. (2006) Movement-related correlates of single cell activity in the interpeduncular nucleus and habenula of the rat during a pellet-chasing task. *Behav. Brain Res.*, **166**, 55–70.

Skaggs, W.E. & McNaughton, B.L. (1996) Replay of neuronal firing sequences in rat hippocampus during sleep following spatial experience. *Science*, **271**, 1870–1873.

Solstad, T., Moser, E.I. & Einevoll, G.T. (2006) From grid cells to place cells: a mathematical model. *Hippocampus*, **16**, 1026–1031.

Steffenach, H.A., Witter, M., Moser, M.B. & Moser, E.I. (2005) Spatial memory in the rat requires the dorsolateral band of the entorhinal cortex. *Neuron*, **45**, 301–313.

Steinvorth, S., Corkin, S. & Halgren, E. (2006) Ecphory of autobiographical memories: an fMRI study of recent and remote memory retrieval. *Neuroimage*, **30**, 285–298.

Strang, G. (1988) *Linear Algebra and its Applications*. Harcourt, Brace, Jovanovich, San Diego.

Swanson, L.W., Wyss, J.M. & Cowan, W.M. (1978) An autoradiographic study of the organization of intrahippocampal association pathways in the rat. *J. Comp. Neurol.*, **181**, 681–716.

Taube, J.S. & Bassett, J.P. (2003) Persistent neural activity in head direction cells. *Cereb. Cortex*, **13**, 1162–1172.

Taube, J.S. & Burton, H.L. (1995) Head direction cell activity monitored in a novel environment and during a cue conflict situation. *J. Neurophysiol.*, **74**, 1953–1971.

Taube, J.S., Muller, R.U. & Ranck, J.B. Jr (1990a) Head-direction cells recorded from the postsubiculum in freely moving rats. II. Effects of environmental manipulations. *J. Neurosci.*, **10**, 436–447.

Taube, J.S., Muller, R.U. & Ranck, J.B. Jr (1990b) Head-direction cells recorded from the postsubiculum in freely moving rats. I. Description and quantitative analysis. *J. Neurosci.*, **10**, 420–435.

Taube, J.S., Kesslak, J.P. & Cotman, C.W. (1992) Lesions of the rat postsubiculum impair performance on spatial tasks. *Behav. Neural Biol.*, **57**, 131–143.

Taube, J.S., Goodridge, J.P., Golob, E.J., Dudchenko, P.A. & Stackman, R.W. (1996) Processing the head direction cell signal: a review and commentary. *Brain Res. Bull.*, **40**, 477–484.

Tsodyks, M.V., Skaggs, W.E., Sejnowski, T.J. & McNaughton, B.L. (1996) Population dynamics and theta rhythm phase precession of hippocampal place cell firing: a spiking neuron model. *Hippocampus*, **6**, 271–280.

Wallenstein, G.V. & Hasselmo, M.E. (1997) GABAergic modulation of hippocampal population activity: sequence learning, place field development, and the phase precession effect. *J. Neurophysiol.*, **78**, 393–408.

Yoshida, M. & Hasselmo, M.E. (2008) Persistent spiking activity in neurons of the postsubiculum (dorsal presubiculum). *Abstr. Soc. Neurosci.*, **34**, 94.13.

Yu, X., Yoganarasimha, D. & Knierim, J.J. (2006) Backward shift of head direction tuning curves of the anterior thalamus: comparison with CA1 place fields. *Neuron*, **52**, 717–729.